JOURNAL OF GUIDANCE, CONTROL, AND DYNAMICS
Vol. 15, No. 2, March-April 1992

Rotor-Pendulum Model for the Perigee Assist Module Nutation Anomaly

A. C. Or*
Hughes Aircraft Company, El Segundo, California 90009

Several years ago, anomalous motion was observed in the flight data from several upper-stage spacecraft known as the Perigee Assist Module that used the STAR 48 series of solid rocket motors. The cause of the anomaly is believed to be due to the asymmetric gas and/or liquid motions in the motor chamber. Control dynamicists have conveniently modeled the motions using an attached point mass on a rotor. In this paper, the nutational stability of a spacecraft modeled as a rotor-pendulum system is examined in the flight parameter region. We show that the simple mechanical model is capable of matching the telemetric angular rates satisfactorily by adjusting a small number of parameters. Although this result strongly supports a type of resonance interaction, a simultaneous match of both the rates and the parameter region of instability does not seem possible. For the simulation of the Perigee Assist Modules, we develop an idealized model, which retains the pertinent features of the pendulum motions, but not certain constraints which may be altered in the actual liquid sloshing.

I. Introduction

ABOUT 10 years ago, a series of upper-stage spacecraft known as Perigee Assist Modules (PAM) was flown. These vehicles consistently displayed a nutation anomaly toward the end phase of the solid rocket motor burn. At the burnout, for some of the spacecraft, the semicone angle grew to as large as 18 deg. The flight data are well established, but the cause of the anomalous motions is not yet fully understood. Many potential destabilizing mechanisms have been ruled out, including the slosh in the fuel tanks.[1] Now it is widely believed that the instability is caused by one, or a combination of both, of the following destabilizing mechanisms: 1) a jet gain moment generated by a gas jet detached from the wall; the moment amplified under the nutation forcing near a resonance condition[2,3]; and 2) a liquid pool of molten slag trapped in the aft annular region of the motor chamber. The slosh motions amplify under a resonant condition and cause nutation to grow in the presence of an axial acceleration. At this point, neither of these two views has provided a conclusive explanation. The similarity of the two views, however, is that both address a type of resonance interaction that is believed to be responsible for the anomalous transition. An understanding of the nature of the instability is considered crucial for both future designs of solid rocket boosters and their attitude control systems.

The jet gain theory proposed by Flandro et al.[2] has received more in-depth treatment than any other theory. The mechanism that these authors proposed is theoretically viable and some experimental investigations have been carried out.[4] On the other hand, the slag theory is supported by some well-established slosh resonance studies in literature.[5,6] Recently, some new evidence emerged that seems to support the slag accumulation hypothesis.[7] This evidence justifies more studies in the area of spacecraft-liquid interactions. In this paper, we make no attempt to discredit either of the two views. In fact, both views become intractable when the realistic physical problem is considered. On the other hand, both views seem to suggest that the instability is a result of an asymmetric motion of the bulk fluid whose mass center motion may be regarded as, in a crude sense, a point mass attached to the spacecraft. Indeed, for control dynamicists, the need for a simple plant model for designing the control system often provides the motivation for adopting this mechanical view of the problem and treating the asymmetric fluid motions as those from an attached point mass. The crucial question concerning system analysts is, therefore, whether a point-mass model is viable. A few years ago, a simple point-mass model that demonstrated resonance interaction of internal mass motion with nutation was studied by Mingori and Yam.[8] In this paper, we are content to extend their approach and to obtain results for a more general situation.

This study serves two purposes. First, it provides a systematic approach for studying the simple mechanical model as a means for reproducing the anomaly behavior based on the comparison with available telemetry data. Of importance is not only matching the dependent variables, but also matching the physical parameter regions of the flight. The latter requirement seems more stringent, but is definitely more important for determining the suitability of the simple model for accurate flight predictions. Second, the simple model may provide the clue for understanding the cause of the anomaly. In this study, the instability parameter region is determined and the stability properties of the simple mechanical systems are analyzed. From a dynamics point of view, the model serves as a good example for illustrating the dynamical properties of a two-mode resonance phenomenon.

It is well known that the inertial oscillations of a spinning liquid have frequencies that fall within the spin speed. The conjecture of a resonance theory (applied to both gas and slag) for the flight anomaly is in fact strongly supported by flight data. A close examination of rate gyro data suggested that the amplification is very likely to be due to a phase locking of two oscillatory modes. The data consistently showed a switch over point in time somewhere between 50–60 s from ignition. Before the switchover, the roll and pitch rates decayed slowly due to the classical jet damping law. After the switching over, the rates grew exponentially until the burnout. In Flandro et al.,[2] growth rate curves were reconstructed from the telemetry data, which show that the growth rate is not constant of time, but rather, it oscillates between zero and an upper envelope curve, where one or more growth rate maxima are observed. The envelope curve appears to increase in some power law fashion of time (more or less quadratic), whose variation and the growth rate fluctuation period are well correlated with the time scale of change of the mass property. The fluctuating growth rate suggests the resonance process, in which the nutation mode locks up with one, or more, of the oscillatory

Received July 24, 1990; revision received July 19, 1991; accepted for publication July 23, 1991.

*Staff Engineer, Dynamics & Control Department, Space & Communication Group, S41, M/S B320, P.O. Box 92919. Member AIAA.

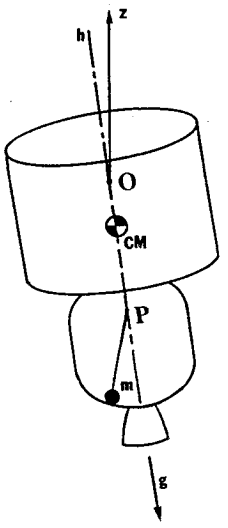

Fig. 1 Geometric configuration of the spacecraft-pendulum system.

modes of the inertial fluid motions during the entire growth period. For a system with slow-varying parameters, the growth rate maximum may not be right at the resonance condition, but is certainly near. Since the mass property of the spacecraft changed substantially throughout the burn, the nutation frequency is expected to change over a substantial range of value.

In this study, we examine the aforementioned process using the simplest mechanical model that is capable of producing such a process. The rigid spacecraft is modeled as a rotor, and the attached oscillator is modeled as a two-degree-of-freedom pendulum system. In general, such a model possesses eight degrees of freedom: three degrees of freedom for the translation of the rotor, three degrees of freedom for the rotation of the rotor, and two degrees of freedom for the pendulum. By decoupling the translation and imposing that spin speed remain constant, we reduce the model to a four-degree-of-freedom system. By further assuming circular symmetry we reduce the two transverse rotation degrees of freedom to one. Thus, we have a three-degree-of-freedom system. For given rotor parameters, only two of these degrees of freedom can interact. A significant simplification arises from the fact that the rotor possesses circular symmetry. In order to preserve this symmetry, we consider two types of pendulums: 1) a single two-degree-of-freedom spherical pendulum, and 2) a pair of planar pendulums each constrained to move in plane containing a transverse axis and the z axis. Both types of pendulums have attached points on the z axis. For the spherical pendulum, the hinge degree of freedom allows the bob to be despun from the rotor. Such a pendulum seems to be appropriate if the fluid is completely inviscid. For the planar pendulums, the center of mass of the pair of bobs also preserves the circular symmetry. The pendulum motions now seem more appropriate for representing the sloshing in a spun fluid since such motions allow interactions with the spin field. Neither of the cases can adequately represent the actual fluid motions, but it appears that each case may represent an extreme behavior of the actual fluid motions. In Sec. II, the equations of motion for case 1 are derived from the first principle using the Newton-Euler approach. The equations for case 2 are obtained from those of case 1 by simple modifications. Of particular interest is obtaining the growth rate relationship as a function of the key parameters of the problem. The growth rate analysis is done in Sec. III. In order to contrast the similarity and difference of the two cases, and to make the analysis more concise, we treat both cases 1 and 2 unifyingly. It will be apparent in the sequel that, even though both cases 1 and 2 are capable of matching the flight telemetry angular rates, neither of these cases can satisfactorily match the flight parameter region and the spacecraft configuration. Simultaneously, case 3, an idealized model, is introduced for matching the flight parameter region. Unfortunately, this case has no correspondence to an actual physical pendulum. The drawback of the physical pendulum models points out the importance of a fluid mechanics solution for the problem. For small parameters, the stability regions are obtained through a simple perturbation method. The advantage of this method is that closed-form expressions are available that provide the first-order approximation for the growth rate. For the general case, however, the results are obtained numerically. In order to test how well the simple model can match the flight data, a flight simulation of a PAM spacecraft, RCA-D, is provided in Sec. IV. The idealized model is used for the demonstration. In Sec. V, we conclude with a few remarks.

II. Mathematical Formulation

Figure 1 shows the geometric configuration of the rotor-pendulum system. The point P represents a U joint with two degrees of freedom. The reference frame is attached to the rotor's center of mass 0. From the Newton-Euler method, the total angular momentum about point 0 and the pendulum angular momentum about point P are given by the following equations:

$$\dot{\boldsymbol{h}}_0 = m\ddot{\boldsymbol{R}}_0 \times \boldsymbol{r} \tag{1a}$$

$$\boldsymbol{\rho} \times (\dot{\boldsymbol{h}}_P - m\ddot{\boldsymbol{R}}_P \times \boldsymbol{\rho}) = 0 \tag{1b}$$

where Eq. (1a) represents the total angular momentum balance of the system about 0 in the absence of external torque. The latter condition is true since the thrust vector passes through 0. Equation (1b) is the angular momentum balance of the pendulum about its pivot P. The position vector of the bob measured from P, $\boldsymbol{\rho}$, is given by $\boldsymbol{\rho} = \boldsymbol{r} - \boldsymbol{r}_P$, where $\boldsymbol{r}$ and $\boldsymbol{r}_P$ are the position vectors of the bob and the pivot, respectively. The variables $\ddot{\boldsymbol{R}}_0$ and $\ddot{\boldsymbol{R}}_P$ are the accelerations of the points 0 and P, respectively, to an inertial viewer; $\boldsymbol{h}_0$ the total angular momentum about 0; $\boldsymbol{h}_P$ the pendulum angular momentum about P; and m the mass of the pendulum. Equations (1) can be further expressed in the more explicit form

$$\boldsymbol{I}\dot{\boldsymbol{\omega}} + \boldsymbol{\omega} \times \boldsymbol{I}\boldsymbol{\omega} + \boldsymbol{r} \times (m_\mu[\ddot{\boldsymbol{r}}] + mg\hat{\boldsymbol{k}}) = 0 \tag{2a}$$

$$\boldsymbol{\rho} \times (m_\mu[\ddot{\boldsymbol{r}}] + mg\hat{\boldsymbol{k}}) = 0 \tag{2b}$$

where $\boldsymbol{\omega}$ is the angular velocity of the rotor, $\boldsymbol{I}$ the rotor's inertia tensor, m_μ the reduced mass given by $m_\mu = mM/(m+M) = m(1-\mu)$, M the rotor mass, and $g = F/(m+M)$, where F is the thrust. The acceleration g must not be confused with the gravitational acceleration. The term $[\ddot{\boldsymbol{r}}]$ represents the relative acceleration between the bob and the point 0 relative to the inertial space. Thus, for a point mass, in general we have

$$[\ddot{\boldsymbol{r}}] = \ddot{\boldsymbol{r}} + 2\boldsymbol{\omega} \times \dot{\boldsymbol{r}} + \boldsymbol{\omega} \times (\boldsymbol{\omega} \times \boldsymbol{r}) + \dot{\boldsymbol{\omega}} \times \boldsymbol{r}$$

In deriving Eqs. (2a) and (2b), the rectilinear equation of motion $(M+m)\ddot{\boldsymbol{R}}_G = F\hat{\boldsymbol{k}}$ and the kinematic condition $\ddot{\boldsymbol{R}}_G = \ddot{\boldsymbol{R}}_0 + \mu\ddot{\boldsymbol{r}}$ have been used. We examine the small perturbational motions about a vertical static equilibrium state $\boldsymbol{r}_s = lq\hat{\boldsymbol{k}}$, $\boldsymbol{\rho}_s = -l\hat{\boldsymbol{k}}$, and $\boldsymbol{\omega}_s = \Omega\hat{\boldsymbol{k}}$, where $q = (Z_0/l - 1)$, and where Z_0 and l are the vertical distance of P above 0 and the pendulum length, respectively. Equations (2a) and (2b) can be linearized about the static state to produce the stability equations,

$$\boldsymbol{I}\dot{\tilde{\boldsymbol{\omega}}} + \boldsymbol{\omega}_s \times \boldsymbol{I}\tilde{\boldsymbol{\omega}} + \tilde{\boldsymbol{\omega}} \times \boldsymbol{I}\boldsymbol{\omega}_s + \hat{\boldsymbol{k}} \times (m_\mu lq[\ddot{\tilde{\boldsymbol{r}}}] - mg\tilde{\boldsymbol{r}}) = 0 \tag{3a}$$

$$\hat{\boldsymbol{k}} \times (m_\mu l[\ddot{\tilde{\boldsymbol{r}}}] + mg\tilde{\boldsymbol{\rho}}) = 0 \tag{3b}$$

The tilde variables represent the small perturbations. Both $\tilde{\boldsymbol{\omega}}$ and $\tilde{\boldsymbol{r}}$ or $\tilde{\boldsymbol{\rho}}$ are on the same order of magnitude. We further define l, the pendulum length, and Ω^{-1}, the inverse of the

spin speed, as the scales of length and time, and we rewrite Eqs. (3a) and (3b) as

$$\dot{\tilde{\omega}} - (\sigma - 1)\hat{k} \times \tilde{\omega} = \epsilon Fr^{-1}(q + 1)\hat{k} \times \tilde{r} \tag{4a}$$

$$\left[\ddot{\tilde{r}} + 2\hat{k} \times \dot{\tilde{r}} + \left(\frac{Fr^{-1}}{1 - \mu} - 1\right)\tilde{r}\right] + q\sigma\tilde{\omega} + Fr^{-1}\epsilon q(q + 1)\tilde{r} = 0 \tag{4b}$$

where

$$\epsilon = \frac{ml^2}{A}, \qquad \sigma = \frac{C}{A}, \qquad Fr = \frac{\Omega^2 l}{g}$$

Here, A and C are the rotor's transverse and axial moments of inertia, respectively. With $\tilde{r} = \tilde{\rho} = l(-\alpha\hat{i} + \phi\hat{j})$ and $\tilde{\omega} = \omega_1\hat{i} + \omega_2\hat{j}$, we can further express Eqs. (4a) and (4b) in the scalar form.

$$\dot{\omega}_1 + (\sigma - 1)\omega_2 = -\epsilon(q + 1)Fr^{-1}\phi \tag{5a}$$

$$\dot{\omega}_2 - (\sigma - 1)\omega_1 = -\epsilon(q + 1)Fr^{-1}\alpha \tag{5b}$$

$$(\ddot{\alpha} - \alpha + 2\dot{\phi}) + \frac{Fr^{-1}}{1 - \mu}\alpha = q[\sigma\omega_1 - \epsilon(q + 1)Fr^{-1}\alpha] \tag{5c}$$

$$(\ddot{\phi} - \phi - 2\dot{\alpha}) + \frac{Fr^{-1}}{1 - \mu}\phi = q[-\sigma\omega_2 - \epsilon(q + 1)Fr^{-1}\phi] \tag{5d}$$

Equations (5a–5d) describe the linear motion of a rotor with a spherical pendulum attached. The equations for the planar case can be obtained easily from Eqs. (5a–5d). To obtain the planar equations we refer back to Eqs. (2a) and (2b) and replace the definitions of m_μ by $m_\mu = mM/(2m + M)$, that of g by $g = F/(2m + M)$, where m is the mass for the individual bob, and that of σ by $\sigma = (1 - \epsilon q^2)C/A$. Accordingly, we also have $\mu = m/(2m + M)$ instead. We observe that Eq. (2a) remains unchanged. To get the counterpart of Eq. (2b), we take the dot product of the equation with $\hat{i}$ to obtain the pendulum motion in the x-z plane. Then we take the dot product of Eq. (2b) with $\hat{j}$ to obtain the pendulum motion in the y-z plane. Thus, Eq. (2b) is modified into two equations describing the motions of two planar pendulums. In component form, the planar equations are similar to those shown in Eqs. (5a–5d), but have been modified as follows: 1) a term $-\epsilon 2q\dot{\alpha}$ is added to the right-hand side of Eq. (5a); 2) a term $\epsilon 2q\dot{\phi}$ is added to the right-hand side of Eq. (5b); 3) the term $2\dot{\phi}$ from the left-hand side of Eq. (5c) is dropped, and a term $2(\mu + \epsilon q^2)\dot{\phi}$ is added to the right-hand side; and 4) the term $-2\dot{\alpha}$ from the left-hand side of Eq. (5d) is dropped, and a term $-2(\mu + \epsilon q^2)\dot{\alpha}$ is added to the right-hand side.

It has been shown numerically that μ is not a sensitive parameter to the stability behavior. Since we are interested in the regime where μ is small ($\approx 10^{-2}$), μ can be set to zero for most practical purposes. However, ϵ, the inertia ratio of the pendulum to the rotor, is a sensitive parameter in the stability behavior, in particular, for the planar model.

The circular symmetry available to Eqs. (5a–5d) and the corresponding planar equations allows us to simplify the system by expressing the set in complex notation. Defining new variables $\omega = \omega_1 + j\omega_2$ and $\Phi = \phi + j\alpha$, combining Eqs. (5a) and (5b), and (5c) and (5d), correspondingly, we obtain the following unified set of equations, which applies to both the spherical and planar case:

$$\dot{\omega} - j(\sigma - 1)\omega = -\epsilon K(q + 1)Fr^{-1}\Phi + jG2\epsilon q\dot{\Phi} \tag{6a}$$

$$\{\ddot{\Phi} - \Phi + 2j[L - G(\mu + \epsilon q^2)]\dot{\Phi}\} + Fr^{-1}\left[\frac{1}{1 - \mu} + \epsilon q(q + 1)\right]\Phi = jK^{-1}q\sigma\omega \tag{6b}$$

Besides the physical parameters ϵ, σ, q, μ, and Fr, the additional parameters in Eqs. (6a) and (6b), K, G, and L, are added to the equations to allow us to treat the three cases unifyingly. The spherical model corresponds to $K = 1$, $G = 0$, and $L = 1$; the planar model corresponds to $K = 1$, $G = 1$, and $L = 0$; and the idealized model corresponds to $K = 10$, $G = 0$, and $L = 0$. The significance of these additional parameters is described as follows. The parameter K serves as a scaling factor for the pendulum amplitude. In both physical models, for a reasonable bob mass, the results show a large pendulum displacement, which is about an order of magnitude larger than the expected physical values. In fact, from the eigenvalue problem of the next section, it can be shown that the ratio of amplitudes of Φ and ω is on the order of $\epsilon^{-1/2}$, which is on the order of 10 or higher. If the nutation angle is a few degrees, the corresponding pendulum angle will be out of range of the small amplitude assumption. The factor K is introduced as a scaling parameter to overcome this problem (see Sec. IV). The factor G is associated with the Coriolis terms, which are present in the planar model but not in the spherical model. As we shall show in next section, these Coriolis terms give rise to an additional effect that is stabilizing. The parameter L is associated with the Coriolis terms that are present in the spherical pendulum equation but not in the planar model. In the following section, we provide the stability analysis for the system of equations (6a) and (6b). The stability properties of the spherical and planar model provides the rationale for us to consider and idealized model for the PAM flight simulation.

III. Growth Rate Analysis

We seek solutions to Eqs. (6a) and (6b) with the following time dependence,

$$\omega = \hat{\omega} \exp j\lambda t, \qquad \Phi = \hat{\Phi} \exp j\lambda t \tag{7}$$

where λ is the eigenvalue to be determined. The characteristic equation of λ is a cubic equation, which is readily solved numerically. However, since the equation depends on quite a number of parameters, for a better physical insight of the stability region, a perturbational analysis seems more beneficial for identifying the dominant behavior and the key parameters. Equations (6a) and (6b) are expressed in a normalized form as follows,

$$\begin{pmatrix} \lambda^* - 1 & -j\epsilon[KP(q + 1) + 2G(Q\lambda^* - R)q] \\ jK^{-1}\sigma Qq & \lambda^{*2} - \beta^2 - \epsilon[2G(Q\lambda^* - R)q^2 + Pq(q + 1)] \end{pmatrix} \times \begin{pmatrix} \hat{\omega} \\ Q^{-1}\hat{\Phi} \end{pmatrix} = 0 \tag{8}$$

where

$$Q = (\sigma - 1 + L - \mu G)^{-1}, \quad P = Q^2 Fr^{-1}, \quad R = Q^2(L - \mu G)$$

$$\lambda^* = Q(\lambda + L - \mu G), \quad \beta^2 = Q^2\left[(L - \mu G)^2 + \left(\frac{Fr^{-1}}{(1 - \mu)} - 1\right)\right] \tag{9}$$

The characteristic equation can be written as

$$(\lambda^* - 1)(\lambda^{*2} - \beta^2) - \epsilon(a_0 + a_1\lambda^* + a_2\lambda^{*2}) = 0 \tag{10}$$

where the coefficients are

$$a_0 = P(Q\sigma - 1)q(q + 1) - 2GR(K^{-1}Q\sigma - 1)q^2$$

$$a_1 = Pq(q + 1) + 2G[K^{-1}Q^2\sigma - (R + Q)]q^2$$

$$a_2 = 2GQq^2 \tag{11}$$

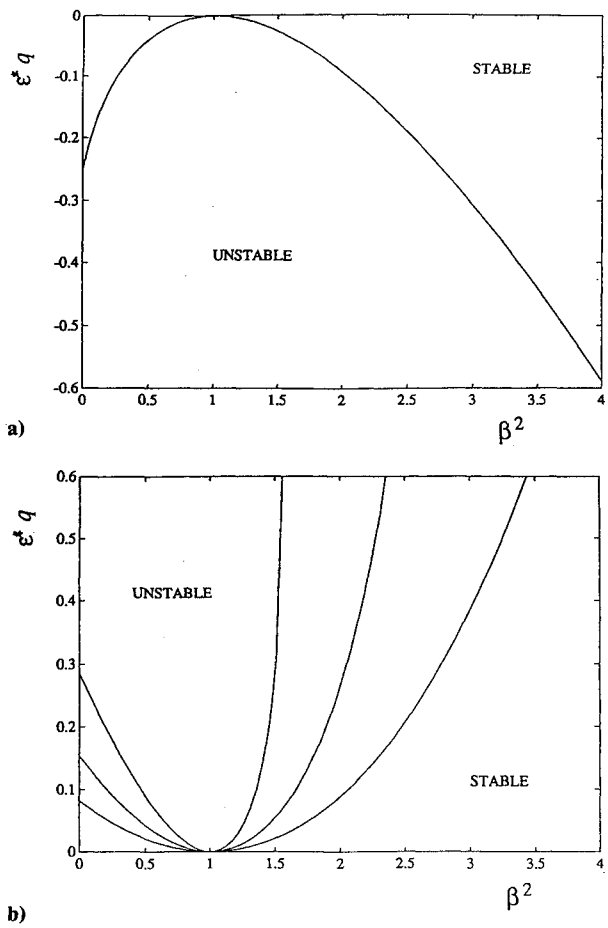

Fig. 2 Stability diagram in the $(\beta^2 - \epsilon^* q)$ plane: a) spherical model; b) idealized model.

For $\epsilon = 0$, the uncoupled characteristic equation gives three roots, that is, $\lambda^* = 1, \pm\beta$. The resonance condition occurs at $\beta^2 = 1$. For $\epsilon \neq 0$ but remains a small positive parameter, our perturbation scheme assumes $\beta^2 = 1 + \Delta$, where the numerical result shows that Δ is on the order of $\epsilon^{1/2}$. We further expand λ^* in a Puiseux series,[9]

$$\lambda^* = 1 + \lambda_0 \epsilon^{1/2} + \lambda_1 \epsilon + \cdots \tag{12}$$

Substituting Eq. (12) into Eqs. (11) and ordering the terms, for the $\mathcal{O}(\epsilon^{1/2})$ balance, we obtain the following simple quadratic equation,

$$2\lambda_0^2 - \left(\frac{\Delta}{\epsilon^{1/2}}\right)\lambda_0 - (a_0 + a_1 + a_2) = 0 \tag{13}$$

which gives

$$\lambda_0 \epsilon^{1/2} = \frac{\Delta}{4} \pm \left[\frac{\Delta^2}{16} + \frac{\epsilon}{2}(a_0 + a_1 + a_2)\right]^{1/2} \tag{14}$$

Instability occurs at resonance when $(a_0 + a_1 + a_2) < 0$. Equation (14) shows how the pair of resonant modes behaves when perturbed near the resonant condition. Equation (14) captures the first-order effects in the frequency shift and the phase locking (if the discriminant changes sign). We shall not carry on the perturbation scheme to the higher order since the algebraic expressions then become fairly complicated. From Eqs. (11), the expression for the sum of coefficients is

$$a_0 + a_1 + a_2 = PQ\sigma q(q + 1) + 2K^{-1}GQ\sigma(Q - R)q^2 \tag{15}$$

The tuned conditions for instability of the spherical model and the idealized model are quite simple. For the spherical model, we set $G = 0$ and $L = 1$ to obtain

$$q(q + 1) < 0 \tag{16}$$

Inequality (16) shows that instability occurs when the rotor's center of mass is between the bob and the pivot. Next, to contrast with the spherical model, we consider an idealized model by setting $G = 0$ and $L = 0$. The reason for considering this model is discussed at the end of this section. For this model, the condition for instability is

$$\frac{1}{(\sigma - 1)} q(q + 1) < 0 \tag{17}$$

Thus, for $\sigma < 1$, instability occurs when either the bob is above the rotor's center of mass or the pivot is below the rotor's center of mass. For $\sigma > 1$, the polarity of the idealized model is the same as the spherical model. The stability condition for the planar model is slightly more complicated due to an additional term. For the planar model, we set $G = 1$ and $L = 0$. Also, for simplicity, we set $\mu = 0$ since we have verified that μ is not a sensitive parameter. The stability criterion at the tuned condition becomes

$$\frac{\sigma}{(\sigma - 1)^3}\{\sigma^2 q + [1 + (\sigma - 1)^2]\} q < 0 \tag{18}$$

Thus, for $\sigma < 1$, the unstable regions correspond to $q > 0$ and $q < -[1 + (\sigma - 1)^2]/\sigma^2$. For $\sigma > 1$, the unstable region corresponds to $0 > q > -[1 + (\sigma - 1)^2]/\sigma^2$.

Figures 2a and 2b show the stability limits on the spherical and the idealized model, respectively, in the $\epsilon^* q$ vs β^2 plane, where we have defined $\epsilon^* = \epsilon P(q + 1)$. Figure 3 shows the stability limits on the $q - \sigma$ plane at the tuned condition $(\beta^2 = 1)$. The shaded area represents the unstable subregions. The regions shaded with lines of positive slope represent the unstable region based on the small amplitude result for $\epsilon < \approx 10^{-3}$. The stability limit for this case is given by the vanishing condition of the inequality (18). The regions shaded with lines of negative slope represent the unstable region for larger ϵ, in this case, we have $\epsilon = 10^{-2}$. The small amplitude stability limit $\sigma = 1.0$ now splits into several subregions.

The simple expression in Eq. (15) contains all of the necessary information of the controlling stability properties. For instability, the right-hand-side expression has to be negative. The expression is comprised of two terms that represent two dominant effects. The first effect, as described by the first term on the right side of Eq. (15), arises from the pull on the rotor at the pivot point from the pendulum bob. The tension force is a function of the state of the pendulum—position and velocity (both magnitude and phase). The state is determined from the sum of the forces and acceleration acting on the bob, which includes the relative acceleration, the Coriolis acceleration, the centripetal acceleration, the axial gravity force, and the tension force. Because of quite a number of forces involved, it is difficult to visualize the pendulum motion by inspection. The first term can be stabilizing or destabilizing, depending on whether it has positive or negative value. The second effect, as described by the second term on the right side of Eq. (15), arises from the effect of the Coriolis reaction acting on the rotor at the pivot point because the pendulums are constrained to move in a planar fashion. From Eqs. (9) and (15), it can be shown easily that this term is always positive. Therefore, its effect is stabilizing. The construction of the idealized model is based on our intuition that, for real liquid sloshing, the Coriolis reaction force on the rotor seems weaker. This means that, for a real liquid, we suggest that the second effect described earlier in the planar model is weaker. As far as the slosh frequency is concerned, we believe that the

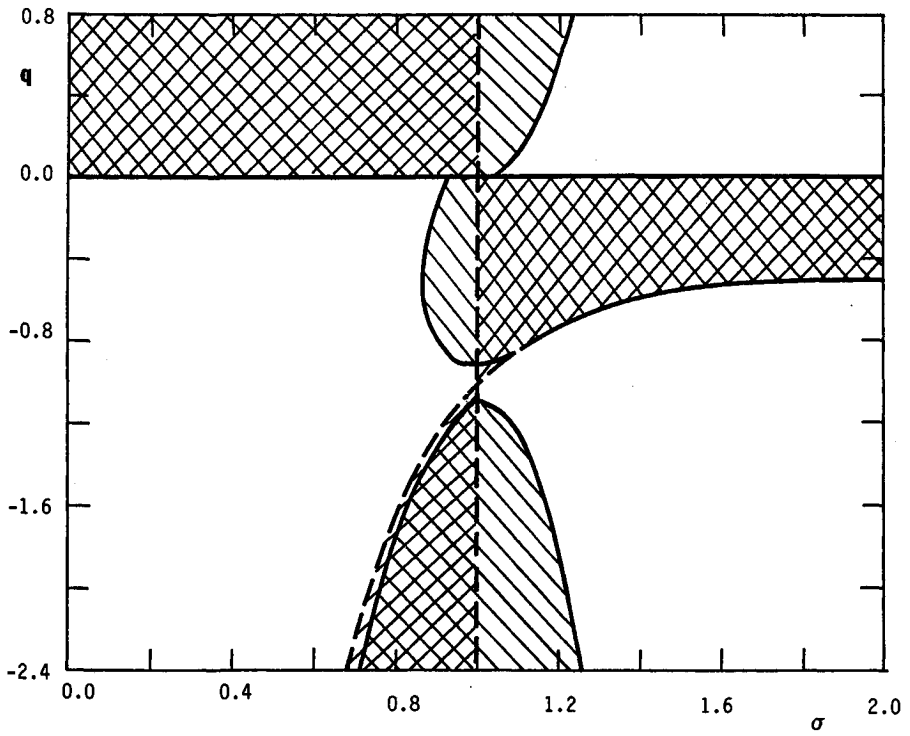

Fig. 3 Stability diagram of the planar model at the tuned condition in the $\sigma - q$ plane (the unstable regions are shaded).

Table 1 Summary of the mass properties of RCA-D during burn

Mass properties	Burn start	Burn end
Mass, lb	7165	2733
Axial moment of inertia, slug-ft^2	525	275
Transverse moment of inertia	2125	570
Center of mass from nozzle exit, ft	6.3	9.4
Thrust magnitude, lbf	16,000	16,000

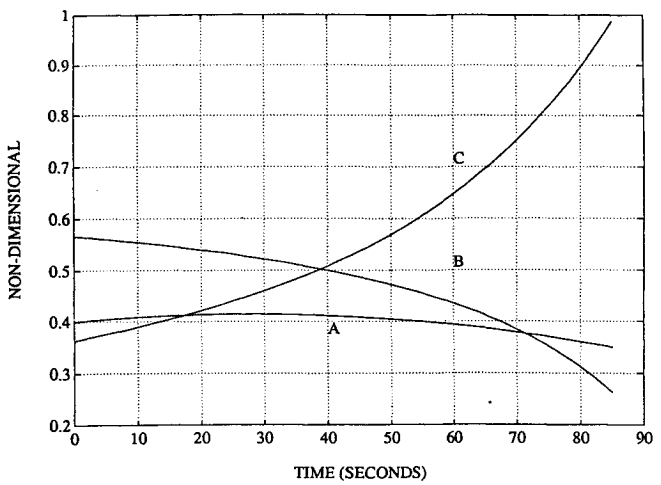

Fig. 4 Time behavior of the assumed pendulum frequency, rotor's body nutation frequency, and assumed pendulum length (maximum scaled to 1).

planar pendulums are more reasonable than the spherical pendulum. Furthermore, for a real liquid, we believe that the asymmetric motion is strongly influenced by the spinning flowfield. This leads us to believe that, for liquid sloshing, the first effect described earlier is more reasonably accounted for by the planar pendulum rather than by the spherical pendulum. Thus, in the idealized model, we have retained the first effect based on the planar pendulum model, and we have neglected the second effect completely. The idealized model corresponds to the case with $G = 0$ and $L = 0$. We believe that the actual liquid behavior is somewhere between those of the idealized pendulums and the planar pendulums. In fact, recently, we have also studied the PAM problem based on a hydrodynamics model[10] using the finite element method. Some preliminary results indeed have indicated that, for a given value of σ occurred in the flight (roughly between 0.3 and 0.5), the stability regions in terms of the axial location of liquid for a given mass of liquid is qualitatively the same as the one given for higher value of σ ($\sigma < 1$) in Fig. 3. This means that, in the liquid model, for roughly 15 lb of liquid and $\sigma \approx 0.5$, we have instability when the liquid is above the spacecraft center of mass, stability when the liquid is slightly below the spacecraft center of mass, and instability again when the liquid is farther below the spacecraft center of mass.

IV. Perigee Assist Module Flight Simulation

Over half a dozen PAM spacecraft have been flown that showed very similar anomalistic behavior. All of these spacecraft had similar mass properties and spin speed. As an example, we simulate the PAM flight anomaly based on the idealized model ($L = 1$, $G = 0$, $K = 10$). Table 1 shows the major flight parameters of the RCA-D spacecraft before and after the rocket motor burn. The spin speed remains fairly constant at 59 rpm. In the flight simulation, these parameters are assumed for the rotor of the model. The burn time is 85 s, during which all of the parameters varied approximately linearly in time. Additional information on the pendulum length and the liquid slosh frequency are required from an independent source. These are assumed quantities, and the following polynomial expression is used for matching the flight data,

$$Fr^{-1} = 1 + a_0 + a_1 t - a_2 t^2, \qquad l = \frac{g}{\Omega^2 Fr} \tag{19}$$

For the simulation, we have used $a_0 = 0.4$, $a_1 = 1.08 \times 10^{-3}$, and $a_2 = 1.96 \times 10^{-5}$. Figure 4 shows three curves that are denoted by A, B, and C and represent the time behavior of

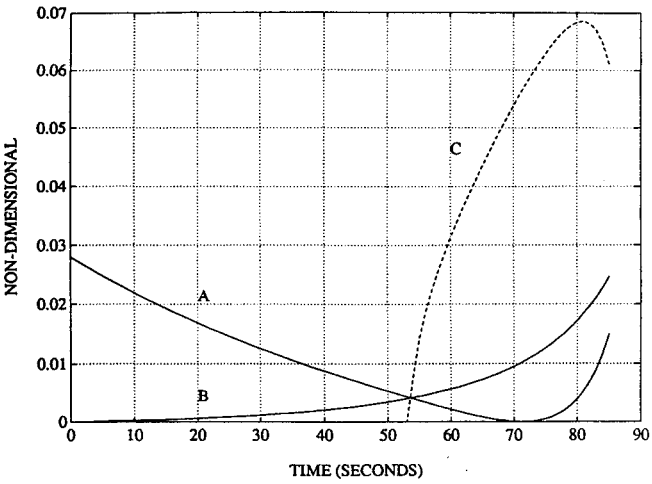

Fig. 5 Time behavior of the simulated value of $\epsilon^* q$, stability limit value of $\epsilon^* q$, and growth rate value of the instability (dotted).

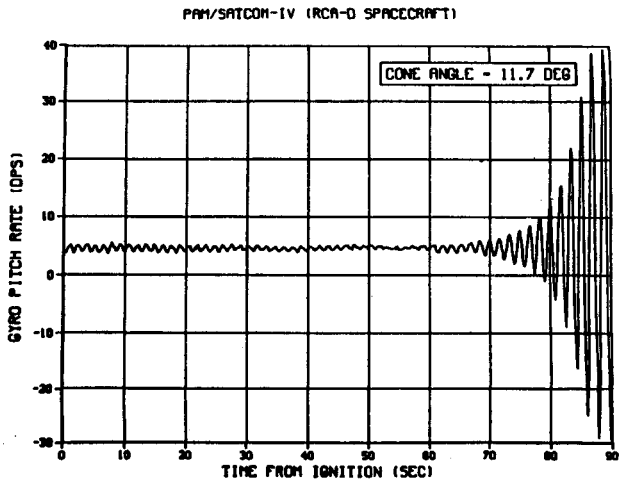

a) Telemetric pitch rate

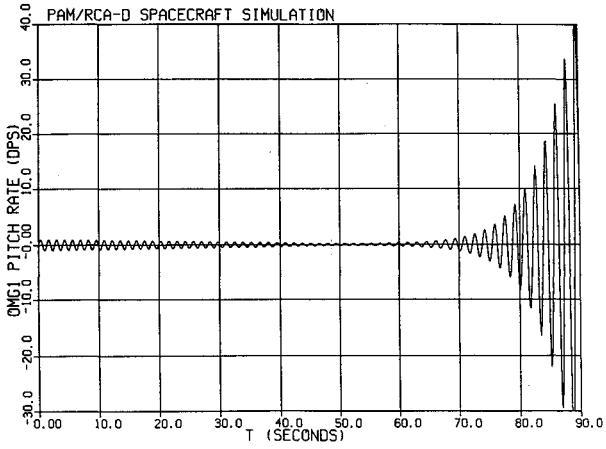

b) Simulated pitch rate

Fig. 6 Comparison of the telemetric pitch rate with the simulated pitch rate under the flight condition of the RCA-D spacecraft.

$(Fr^{-1} - 1)$, $(\sigma - 1)^2$, and I/I_m, respectively, where $I_m = 3.5$ ft. Based on our assumption, the tuned pendulum (resonance) condition occurs at about 70 s after the start of the burn, where the curves A and B cross each other. As mentioned before, at this condition, a pair of imaginary roots (purely oscillatory modes) merges and a pair of complex conjugate roots form as this condition is crossed. Figure 5 shows a family of curves, again denoted by A, B, and C, which represent the stability limit of $\epsilon^* q$ in the model, the simulated flight $\epsilon^* q$ value, and the growth rate of the instability, respectively. The growth rate is normalized, based on the definition in Eqs. (9). The regions above curves A and B are unstable. Thus, the curves show that the instability starts at about 53 s after the burn begins. Curve C shows a peak growth rate of 0.07 approximately. Converting this value back to the dimensional by multiplying by $(1 - \sigma)\Omega$, we obtain a value of 0.224/s, which corresponds to a time constant of about 4.5 s, which is roughly the observed burnout value.

Next, we develop a quasistatic simulation based on the same model for comparison with the flight telemetry data. Rewriting Eqs. (6a) and (6b) in the matrix form, we have

$$\frac{\mathrm{d}}{\mathrm{d}t}\begin{pmatrix}\omega\\ \Phi\\ \dot{\Phi}\end{pmatrix} = \begin{bmatrix} j(\sigma-1) & -\epsilon(q+1)Fr^{-1}K & 0\\ 0 & 0 & 1\\ j\dfrac{(\sigma q)}{K} & \left\{1-Fr^{-1}\left[\dfrac{1}{1-\mu}+\epsilon q(q+1)\right]\right\} & 0\end{bmatrix}\begin{pmatrix}\omega\\ \Phi\\ \dot{\Phi}\end{pmatrix} \tag{20}$$

Now the state matrix has slow time-varying elements based on the bounding parameters given in Table 1. Figure 6a shows the telemetric pitch rate, and Fig. 6b shows the corresponding simulation result. The dissipative damping effect is not included. However, the jet damping moment has been added as an external torque. The following nondimensional expression has been added to the right-hand side of Eq. (20) during the simulation,

$$M_J = -0.7\,\frac{\dot{m}(L_2^2 - L_1^2)}{A\Omega}\begin{pmatrix}\omega\\ 0\\ 0\end{pmatrix} \tag{21}$$

where L_1 and L_2 are the distance between the rotor center of mass and the top end wall of the chamber and the distance between the rotor center of mass and the nozzle exit plane, respectively. The measure L_2 is given in Table 1 and $L_2 - L_1$ is assumed to be constant at 5 ft. It is important to notice that there is no way to produce the behavior of Fig. 6b without time-varying mass property in the system. We also notice that the fact that the model's growth rate shown in Fig. 5 rises from zero to a maximum is consistent with that shown in the telemetric data (see Ref. 2). Such a behavior is a strong evidence for the occurrence of phase locking in the PAM anomaly.

V. Discussion

The two physical pendulum models studied in this paper not only represent the simplest mechanical point mass systems that can allow a resonance-type interaction with nutation, but are also considered to be valid first-order models of the liquid sloshing. Even for the simple mechanical models, the general stability problems are quite complex. So far, our study has been limited to the linear stability analysis. Since the equilibrium point is nonhyperbolic, a more general study may be required to address the nonlinear stability issue, such as the construction of the global behaviors. We have demonstrated that, based on the quasistatic approximation, the pendulum model can indeed simulate the flight data, that is, the results can match the telemetric angular rates by adjusting the pendulum parameters. These parameters are 1) the Froude number, which has been identified for determining the pendulum frequency, and thus the tuned condition; 2) the axial location of the pendulums, which determines the strength of the coupling between the pendulums and the rotor; and 3) the inertia ratio, which, besides determining the tuned condition, also affects the coupling significantly in the planar model. The three types of pendulum systems we considered have shown how altering

the force balances can result in different stability behaviors. Clearly, the pendulum parameters in the unstable region of both the spherical model and the planar model do not match successfully with those inferred from the flight data. Their stability properties, however, allow us the understanding to construct an idealized pendulum model that has more desirable properties. They also provide motivation for considering the much more difficult problem of a coupled hydrodynamic model to better quantify their important force balances.

Of more general interest is that the dynamical properties of the instability appear to violate simple intuition. Without the rotation and with the follower gravity field replaced by the conservative gravity field, the stability behavior of the two-body problem is rather simple. Since the translational degrees of freedom are decoupled, our equations of motion are dynamically equivalent to the ones with the rotor center of mass fixed inertially. For a conservative nonrotating system, the potential energy provides the sole measure of the stability. Even for the rotating system in a conservative force field, the potential energy principle still applies (by including the centrifugal potential). In this problem, however, the follower thrust does not seem to have a potential. Simple arguments based on the potential energy are generally invalid. For example, in the spherical model, the rotor may still be stable even though the pivot point of the pendulum is above the rotor's center of mass. By kinematic arguments, such a configuration has another state of even lower potential energy. On the other hand, for the planar model, the rotor may be unstable even if its center of mass is above the pivot. Of particular interest in the result of the planar pendulum model is that the configuration can be unstable under thrust when both pivot and bob are below the rotor's center of mass. From a potential energy point of view, such an unstable situation is contrary to the intuition.

VI. Conclusions

A stability problem of a three-degree-of-freedom rotor-pendulum spacecraft model has been studied in the parameter region of the flight anomaly of the PAM. The major conclusion of this study is that the simulation results support the theory of resonance interactions as the cause for the PAM anomaly. The telemetric body angular rates can be matched satisfactorily by adjusting a few key parameters. Explanations have been given for the discrepancy between the flight and the model parameters in the instability region. In particular, we suggest that the anticipated liquid sloshing may have a quantitatively different force balance from the mechanical pendulums, even though the qualitative effects of the sloshing can be accounted for by the pendulum motions. The desired force balance for the PAM flight simulation is reflected from the construction of the idealized pendulum model. The rotor-pendulum models considered are important not only for modeling the first-order sloshing effects in the spacecraft, but also for providing the insight for later developments of more complex dynamical models.

Acknowledgments

The flight telemetry data for the PAM spacecraft provided by the McDonnell Douglas Astronautics Company is gratefully acknowledged. I am grateful to A. D. Challoner for providing me the check of the governing equations using the symbolic software *Sd/fast* and *Mathematica.*

References

[1]Hill, D. E., and Baumgarten, J. R., "Dynamic Simulation of Spin-Stabilized Spacecraft with Sloshing Fluid Stores," *Journal of Guidance, Control, and Dynamics,* Vol. 11, No. 6, 1988, pp. 597–599.

[2]Flandro, G. A., et al., "Fluid Mechanics of Spinning Rockets," Air Force Rocket Propulsion Lab., TR-86-072, 1987.

[3]Flandro, G. A. et al., "Flow-Induced Nutation Instability Mechanism in a Spinning Solid Propellant Rockets," Air Force Rocket Propulsion Lab., TR-89-084, 1990.

[4]Knappenberger, A. S., "Simulating the Vortex in a Spinning Rocket," Phillips Lab., AL-TR-90-070, May 1991.

[5]Abramson, H. N., "The Dynamic Behavior of Liquids in Moving Containers," NASA SP-106, 1966.

[6]Stewartson, K., "On the Stability of a Spinning Top Containing Liquid," *Journal of Fluid Mechanics,* Vol. 5, 1959, pp. 577–592.

[7]Arnold Engineering Development Center, private communication, 1989.

[8]Mingori, D. L., and Yam, Y., "Nutational Instability of a Spinning Spacecraft with Internal Mass Motion and Axial Thrust," *Proceedings of the AIAA Astrodynamics Conference,* AIAA, New York, 1986, pp. 367–375.

[9]Lancaster, P., *The Theory of Matrices,* Academic, London, 1969.